ELSEVIER

Catalysis Today 57 (2000) 261–266

CATALYSIS TODAY

www.elsevier.com/locate/cattod

Preparation and characterization of high surface area niobia, ceria–niobia and ceria–zirconia

Roberta Brayner [a,b,*], Dragos Ciuparu [a], Gilberto M. da Cruz [b], Françoise Fiévet-Vincent [a], François Bozon-Verduraz [a]

[a] *Laboratoire de Chimie des Matériaux Divisés et Catalyse, Université Paris 7, 2 Place Jussieu, 75251 Paris Cedex 05, France*
[b] *Departamento de Engenharia de Materiais, Faculdade de Engenharia Quimica de Lorena, Rod. Itajuba-Lorena, Km 74.5, 12600-000 Lorena, SP, Brazil*

Abstract

Niobia, zirconia, ceria–niobia and ceria–zirconia oxide nanoparticles are prepared by soft chemical routes and show valuable textural properties. The pore volume and specific surface area keep significant values even after calcination at 873 K. According to DRX and STEM-EDX measurements, solid solutions are obtained in the case of ceria–zirconia, whereas separate phases are identified in ceria–niobia; in the latter case, however, UV–Vis diffuse reflectance spectroscopy shows also the formation of defects (color centers) arising from a partial dissolution at the interface of the oxide phases.

Keywords: Ceria–zirconia; Ceria–niobia; Digestion; Anchoring; Diffuse reflectance

1. Introduction

During the last decade, niobium oxide has received a growing attention in the field of catalysis; investigations have concerned various niobium–oxygen species and applications: (i) *bulk* niobia, generally in the acidic form (Nb_2O_5, xH_2O) [1] as the *active phase* [2]; (ii) *bulk* niobia as a *support* [3–5]; (iii) *bulk mixed* oxides of niobia (solid solutions or definite compounds) as active phase or support [3]; (iv) niobia *supported* on various oxides (alumina, silica, titania, magnesia) [6–10]; (v) niobia as *additive*, often on supported transition metal oxides catalysts [5].

Our work is mainly devoted to the preparation and characterization of high surface area niobia and of ceria–niobia mixed oxides; in opposition with zirconia-based composites, niobia-based mixed oxides have received little attention. The present paper deals with (i) the preparation by a soft chemical route of high surface area samples, resistant to sintering, with controlled porosity; (ii) their characterization by complementary techniques such as XRD, DTA–TGA and UV–Vis–NIR spectroscopies. For comparison, some results obtained with ceria–zirconia composites are presented.

2. Experimental

Nb_2O_5 (HY-340) and ammonia complex of Nb were kindly supplied by CBMM (Companhia Brasileira de Metalurgia e Mineração, Brazil); $ZrO(NO_3)_2$ was obtained from Aldrich.

Pure niobia was prepared by *digestion* from an ammonium complex of niobium in an aqueous hydrazine solution for 144 h at 373 K and subsequent calcination

* Corresponding author.

0920-5861/00/$ – see front matter
PII: S0920-5861(99)00335-1

at 723 K for 6 h under flowing oxygen; zirconia was obtained from zirconyl nitrate according to the same procedure. The specific surface areas are 150 m^2/g for niobia and 290 m^2/g for zirconia.

The ceria–niobia samples were prepared by either *digestion* or *anchoring* [11]. The digestion procedure was carried out as above by mixing solutions of ammonium–cerium(IV) nitrate and ammonium complex of niobium. In the anchoring procedure, niobia was heated in a toluene solution of Ce(IV) acetylacetonate for 2 h at 383 K; the solid obtained after filtering and washing by toluene at room temperature was dried at 323 K overnight and calcined at 873 K for 6 h under flowing oxygen. The same procedures were used to prepare ceria–zirconia samples (4–30%wt. CeO_2). The specific surface areas range between 60 and 80 m^2/g after calcination at 873 K for all samples.

Chemical analyses were carried out at the Materials Engineering Department, DEMAR/FAENQUIL, Lorena, SP, Brazil by inductively coupling plasma-atomic emission spectroscopy (ICP-AES).

X-ray powder diffraction (XRD) patterns were recorded using a CoKα radiation. The diffractometer was calibrated using a standard Si sample. The counting time was 30 s per step of 0.05° 2θ. The mean crystallite size was estimated using the Scherrer equation, after computer fitting using pseudo-voigt function (software Profile-SOCABIM Diffract-At).

TEM measurements were performed with a JEOL 100CXII operating at 100 kV.

X-ray energy dispersive spectrometry (EDX) was performed using a LINK AN 10 000 system (Si–Li detector) connected to a JEOL JEM CXII transmission electron microscope operating at 100 kV and equipped with an ASID 4D scanning device (STEM mode). The X-rays emitted from the specimen upon electron impact were collected in the 0–20 keV range for 200–400 s. Atomic compositions (%) were obtained with the 2LINK program (RTS-2/FLS).

UV–Vis–NIR diffuse reflectance spectra (DRS) were recorded on a Cary 5E spectrophotometer equipped with a PTFE-coated integration sphere.

Specific surface areas (S_g) of the materials after calcination were determined by physisorption of nitrogen at 77.3 K and calculated using the BET method; the pore size distribution was obtained from a QUANTACHROME-Autoscan 33 mercury porosimeter at the National Institute of Spatial Research (INPE, Cachoeira Paulista SP, Brazil).

DTA–TGA measurements were performed on a SETARAM thermobalance.

Table 1
Preparation methods and composition of the samples

Sample	Preparation method	CeO_2 (%)	ZrO_2 (%)	Nb_2O_5 (%)
CEZR-1	Anchoring	5.8	94.2	–
CEZR-2	Digestion	9.8	90.2	–
CEZR-3	Digestion	18.0	82.0	–
CEZR-4	Digestion	27.0	73.0	–
CENB-1	Digestion	8.5	–	91.5
CENB-2	Digestion	20.8	–	79.2
CENB-3	Anchoring	5.9	–	94.1

3. Results and discussion

Table 1 collects the compositions of all samples prepared by anchoring or digestion.

3.1. Ceria–niobia

XRD patterns of the samples after calcination at 873 K (Fig. 1) show the presence of cubic ceria in ceria-richest samples (CENB-1 and CENB-2) but not in a CENB-3 (lowest Ce content). As no noticeable shift is detected on the niobium oxide peaks, niobium ions were not substituted by significant amounts of cerium in digested samples. This can be explained by the reduction of Ce^{4+} to Ce^{3+} in hydrazine (a base and a reducing agent), which may disturb the co-precipitation and produce Ce^{3+} ions, of larger size than Ce^{4+}: (ionic radii: 1.03 and 0.92 Å, respectively), more difficult to introduce in the niobia lattice (ionic radius of Nb^{5+}: 0.69 Å). On the other hand, in the anchored sample, the presence of ceria peaks is not detected, may be due to a lowest Ce content.

The STEM-EDX analysis (Table 2) confirms the DRX results: (i) spherical ceria nanoparticles are observed on niobia slabs; (ii) this appears also in the *local* Ce/Nb atomic ratios measured in different areas of the same sample: these values are scattered, which indicates the presence of Ce-rich and Ce-poor areas. In addition the *global* atomic ratio averaged from five

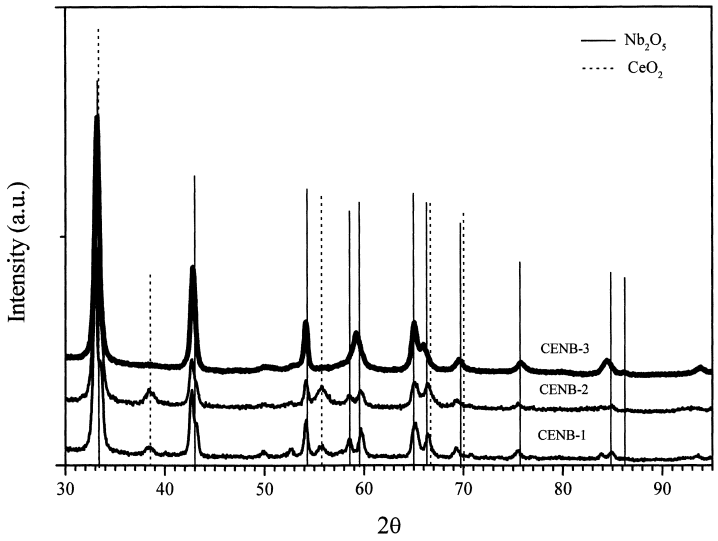

Fig. 1. XRD patterns of *ceria–niobia* samples after calcination at 873 K.

scanning determinations is higher than that measured by ICP-AES analysis (Table 2).

The DRS spectra of *pure oxides* (Fig. 2) are characterized by a strong absorption in the UV range due to the interband transition, which allows the estimation of the band gap width: 3.4 eV for niobia and 3.1 eV for ceria (spectra B and A, absorption threshold near 360 and 400 nm, respectively); the *mixed oxides* (Fig. 2, spectra E, F, G) show an additional absorption in the visible range (400–600 nm); this feature is not observed on *mechanical mixtures* of ceria and nio-

Table 2
Atomic Ce/Zr and Ce/Nb ratios averaged from STEM-EDX and comparison with the bulk chemical composition from ICP-AES

Sample	Atomic ratios		
	ICP-AES	STEM-EDX	
		Global	Local
CEZR-3	0.13	0.17	0.15 0.17 0.16 0.19 0.19
CENB-2	0.16	0.54	0.12 0.5 0.24 1.3

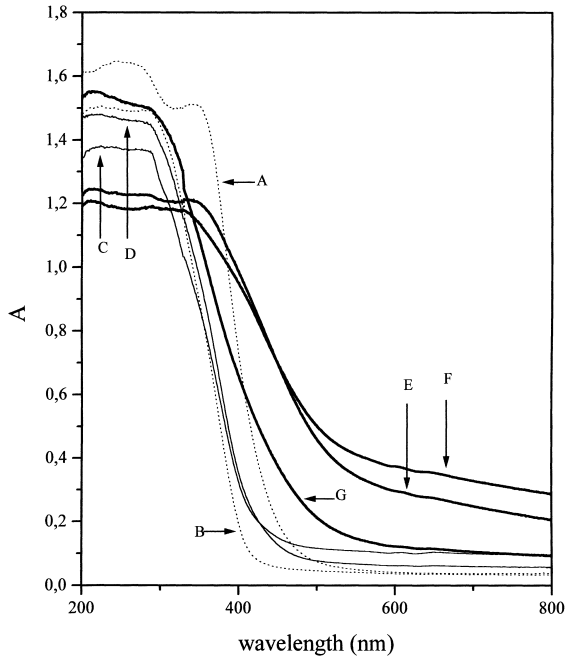

Fig. 2. DRS spectra of *ceria–niobia* samples: (A) CeO_2; (B) Nb_2O_5; (C) 10% CeO_2–Nb_2O_5 (mec. mixture); (D) 20% CeO_2–Nb_2O_5 (mec. mixture); (E) CENB-1; (F) CENB-2; G-CENB-3.

bia (spectra C and D); as a consequence, the *mixed oxides* appear yellowish-brown whereas pure ceria and mechanical mixtures are light yellow. The NIR range show also harmonics and combination bands of OH groups and of metal–oxygen–metal bridges (not shown). The absorption in the visible range may be ascribed to defects resulting from a *partial dissolution occurring at the interface* of the two oxide phases. According to the *point defect model* [12], substitution of a Nb^{5+} ion by Ce^{4+} in the niobia network adds a negative charge which may be compensated by an oxygen vacancy trapping one electron; substitution of a Ce^{4+} ion by Nb^{5+} in the ceria network brings a positive charge which may be compensated by the formation of Ce^{3+} ions; it is known that the presence of Ce^{3+} ions in ceria gives rise to an absorption band near 650 nm [13,14], in addition, preliminary EPR results indicate that paramagnetic species are present. It is relevant to note that UV–Vis DRS is a sensitive tool because of the high extinction coefficients of the charge transfer transitions involved when defects and impurities are present [12].

Table 3 shows the particle size and the total pore volume after calcination. All niobia-containing materials are mainly mesoporous (10^2 Å$<D_P<10^3$ Å) after calcination at 873 K but the total pore volume (cm^3/g) decreases when the sample is prepared by digestion, suggest that no co-precipitation has occurred during the digestion process. On the other hand, the sample prepared by anchoring presents a total pore volume very close to that of HY-340 (Nb_2O_5– CBMM).

Table 3
Particle size and total pore volume of ceria–niobia samples after calcination at 873 K

Sample	Total pore volume (cm^3/g)	D_P (nm) DRX	
		CeO_2	Nb_2O_5
CENB-1	0.077	5.8	14.2
CENB-2	0.095	6.4	15.8
CENB-3	0.551	–	14.6
Nb_2O_5–HY-340	0.592	–	19.1
CeO_2	0.371	10.7	–

3.2. Ceria–zirconia

The pure zirconia prepared by digestion is amorphous and transforms into the tetragonal form at about 1023 K and into the monoclinic form at about 1473 K; in *mixed ceria–zirconia* samples, XRD patterns (Fig. 3) show clearly that CeO_2–ZrO_2 solid solutions are formed by substitution of Zr^{4+} ions by Ce^{4+} in the zirconia lattice, as evidenced by the shift of the zirconia peaks towards small angles (Ce^{4+} is about 20% larger than Zr^{4+}); such substitution leads to the lowering of the crystallization temperature of

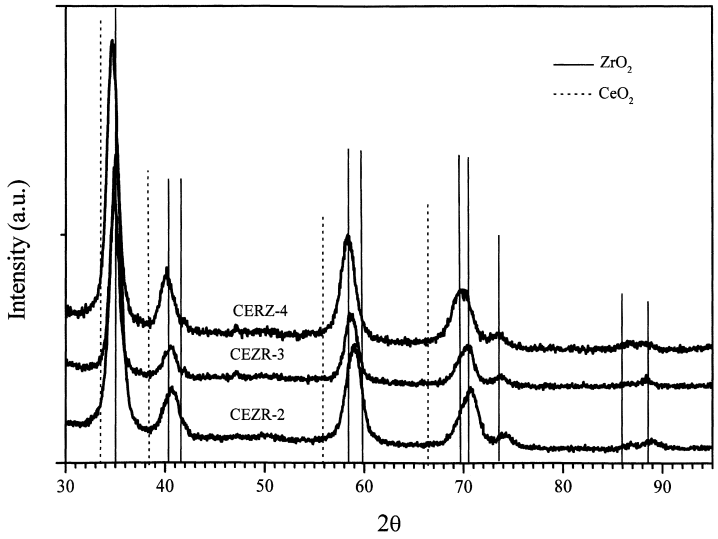

Fig. 3. XRD patterns of *ceria–zirconia* samples after calcination at 873 K.

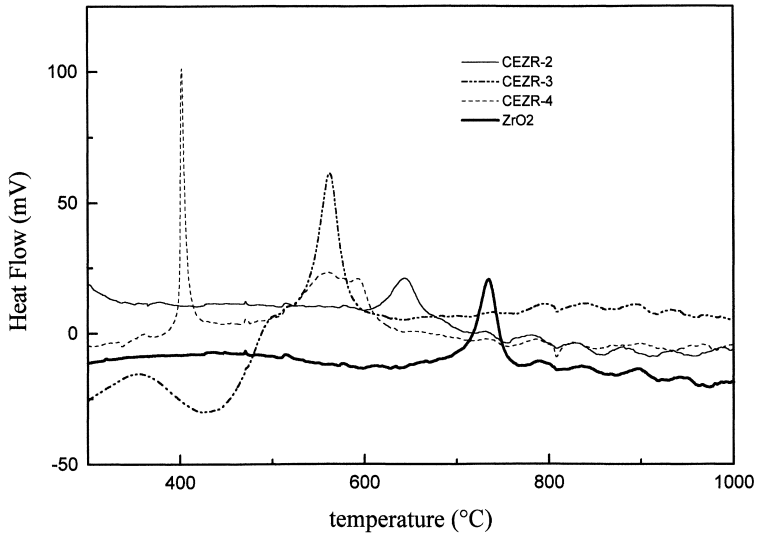

Fig. 4. DTA–TGA experiments of *ceria–zirconia* samples.

the tetragonal form of zirconia down to 673 K. In addition, DTA–TGA experiments (Fig. 4) under flowing N_2 at 1273 K show that, tetragonal and monoclinic zirconia structures are present in the mixed sample containing 27% CeO_2 (CEZR-4) whereas the latter (monoclinic) appear at 1473 K when ceria is absent. Hence the presence of Ce^{4+} ions favors the amorphous → tetragonal and tetragonal → monoclinic transformations. The STEM-EDX analysis confirms the DRX results: (i) spherical nanoparticles of ceria–zirconia are observed; (ii) the *global* and the *local* results are very close to values from ICP-AES analysis (Table 2). The formation of ceria–zirconia solid solutions has been reported by several authors [15,16] including when this composite is loaded with platinum [16]; introduction of zirconium ions into the ceria lattice as well as the reverse situation was observed, depending on the preparation method and on the cerium/zirconium ratio. In the present work, the main result is the synthesis of solid solutions of ceria in zirconia as *nanoparticles* at 873 K.

Fig. 5 presents the DR spectra of pure and mixed oxides; the band gap width of zirconia (about 4.5 eV) is quite different from that of ceria (3.1 eV) and the spectra of mechanical mixtures of these oxides (spectra C and D) are composed of two separate absorption thresholds located near the thresholds of each components. On the other hand, the spectra of mixed oxide (E and F) present only one absorption threshold, without absorption below 450 nm; substitution of isovalent cations (Ce^4, Zr^{4+}) should not, indeed, give rise to the

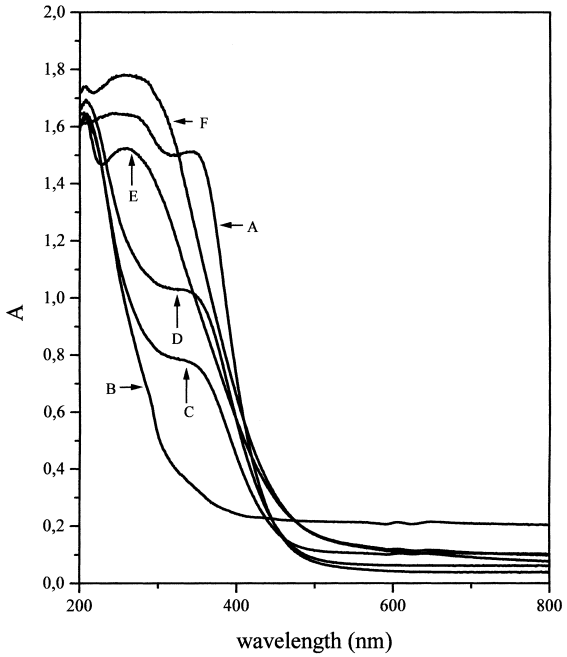

Fig. 5. DRS spectra of *ceria–zirconia samples*: (A) CeO_2; (B) ZrO_2; (C) 10% CeO_2–ZrO_2 (mec. mixture); (D) 30% CeO_2–ZrO_2 (mec. mixture); (E) CEZR-2; (F) CEZR-4.

Table 4
Particle size and total pore volume of ceria–zirconia samples after calcination at 873 K

Sample	Total pore volume (cm^3/g)	Mean crystallite size (nm) XRD
CEZR-1	0.266	4.2
CEZR-2	0.397	6.5
CEZR-3	0.405	8.0
CEZR-4	0.434	7.0
CeO_2	0.371	10.7
ZrO_2	0.492	Amorphous

formation of defects (color centers); this gives another support to the introduction of Ce^{4+} in the zirconia lattice.

Table 4 shows the particle size and the total pore volume; the total pore volume of the ceria–zirconia samples prepared by digestion is higher than that of ceria–niobia samples prepared in the same conditions; this is explained by the extensive formation of solid solutions in the former case.

4. Conclusion

The digestion in hydrazine, a soft chemical route, is an interesting procedure to design pure zirconia and niobia presenting valuable textural properties even after calcination at 873 K. In the case of ceria–zirconia, nanoscale crystallites of solid solutions are formed. In ceria–niobia composites, structural studies show that ceria and niobia are present as separate phases but UV–Vis DRS suggests that a solid solution is formed at the interface of the oxide phases. The above results emphasize the interest of this technique for gaining more insight into the properties of composite oxides.

Acknowledgements

The authors are indebted to *CNPq, Brazil* for the support and financial resources. Thanks to Ph.D. J.A.J. Rodrigues, J.B.F. Jofre and D.J.A. de Souza (National Institute of Spatial Research, INPE, Cachoeira Paulista SP, Brazil) for the porosimetry measurements. Thanks to J.R. Barbosa (Materials Engineering Department, DEMAR/FAENQUIL, Lorena, SP, Brazil) for the ICP-AES analysis. The authors are also grateful to P. Beaunier (Laboratoire de Réactivité de Surface-Univ. Paris VI) for the STEM-EDX analysis and M.J. Vaulay and G. Cheguillaume for their technical assistance.

References

[1] T. Ushikubo, T. Iizuka, H. Hattori, K. Tanabe, Catal. Today 16 (1993) 291.
[2] A. Fiorentino, P. Cartraud, P. Magnoud, M. Guisnet, Appl. Catal. A 89 (1992) 143.
[3] J.C. Vedrine, G. Coudurier, A. Ouqour, P.G. Pries de Oliveira, J.C. Volta, Catal. Today 28 (1996) 3.
[4] J.M. Jehng, A.M. Turek, I.E. Wachs, Appl. Catal. A 83 (1992) 179.
[5] I.E. Wachs, J.M. Jehng, G. Deo, H. Hu, N. Arora, Catal. Today 28 (1996) 199.
[6] J.M. Jehng, I.E. Wachs, Catal. Today 16 (1993) 417.
[7] N. Ichikuni, M. Shirai, Y. Iwasawa, Catal. Today 28 (1996) 49.
[8] J. Datka, A.M. Turek, J.M. Jehng, I.E. Wachs, J. Catal. 135 (1992) 186.
[9] S. Hasegawa, H. Aritani, M. Kudo, Catal. Today 16 (1993) 371.
[10] R.M. Pittman, A.T. Bell, J. Phys. Chem. 97 (1993) 12 178.
[11] A. Bensalem, F. Bozon-Verduraz, M. Delamar, M.G. Bugli, Appl. Catal. A 121 (1993) 81.
[12] P.A. Cox, Transition Metal Oxides — An Introduction to their Electronic Structure and Properties, International Series of Monographs on Chemistry 27, Clarendon Press, Oxford, 1995.
[13] A. Rakai, A. Bensalem, J.C. Muller, D. Tessier, F. Bozon-Verduraz, in: L. Guczi et al. (Eds.), New Frontiers in Catalysis, Proceedings of the 10th International Congress on Catalysis, 1992, Budapest, Hungary, 1993, Elsevier, Amsterdam, 1875.
[14] C. Binet, A. Badri, J.C. Lavalley, J. Phys. Chem. 98 (1994) 6392.
[15] .G. Balducci, P. Fornasiero, R. Di Monte, J. Kaspar, S. Meriani, M. Graziani, Catal. Lett. 33 (1995) 193.
[16] C.E. Hori, H. Permana, K.Y.S. Ng, A. Brenner, K. More, K.M. Rahmoeller, D. Belton, Appl. Catal. B 16 (1998) 105.